RESEARCH PAPER

High-Performance Hybrid Asymmetric Supercapacitors with rGO/α-Fe_2O_3 and rGO/TiO_2 Nanocomposites

Zeinab Abbasali KarajAbad[1], Adrine Malek Khachatourian[1,*], Mohammad Golmohammad[2], Ali Nemati[1]

* *khachatourian@sharif.edu*

[1] Department of Materials Science and Engineering, Sharif University of Technology, Tehran, Iran
[2] Renewable Energy Department, Niroo Research Institute (NRI), Tehran, Iran

Received: November 2024 **Revised: February 2025** **Accepted: March 2025**
DOI: 10.22068/ijmse.3791

Abstract: *Hybrid asymmetric supercapacitors using distinct cathode/anode materials offer enhanced energy density by expanding operational potential windows compared to symmetric configurations. This work synthesised rGO/α-Fe_2O_3 and rGO/TiO_2 nanocomposites via the hydrothermal method for hybrid asymmetric supercapacitors applications. A field emission scanning electron microscope (FESEM) revealed a uniform distribution of spherical α-Fe_2O_3 and TiO_2 nanoparticles on rGO sheets. The X-ray diffractometry (XRD) analysis confirmed the presence of the hematite and anatase in the rGO/α-Fe_2O_3 and rGO/TiO_2 nanocomposites, respectively. Additionally, in the XRD spectra of both nanocomposites, a broad peak corresponding to the (002) crystalline planes of rGO was observed. Electrochemical testing showed specific capacities of 130 F/g (rGO/α-Fe_2O_3) and 253 F/g (rGO/TiO_2) at 5 mV/s in 1 M KOH. The assembled hybrid asymmetric supercapacitors (rGO/α-Fe_2O_3//rGO/TiO_2) achieved a 1.6 V operational potential window. Power density and energy density of 1066 W kg^{-1} and 9.7 Wh kg^{-1} were achieved at a current density of 1 A/g, respectively.*

Keywords: *Hybrid asymmetric supercapacitor, Graphene oxide, rGO/α-Fe_2O_3, rGO/TiO_2, Nanocomposite.*

1. INTRODUCTION

The increasing need for renewable energy and the demand for practical energy storage devices have spurred extensive research into creating high-performance supercapacitors. Supercapacitors offer advantages over traditional batteries, including elevated power density, rapid charge/discharge rates, and longer stability [1, 2]. Among the various types of supercapacitors, asymmetric supercapacitors (ASCs) have garnered considerable attention due to their capability to merge the excellent energy density of batteries with the elevated power density of traditional supercapacitors [3, 4]. ASCs utilize two electrode materials: a battery-type material with high energy density and a capacitive-type material with high power density. This configuration leverages the complementary properties of the two materials, resulting in improved overall device performance [5, 6]. The various ASCs are conducting polymer-carbon, metal oxide-carbon, and hybrid ASCs. Hybrid ASCs combine different types of battery-type and capacitive-type materials to optimize performance. These hybrid systems offer a versatile approach to designing high-performance ASCs. Integrating different materials in hybrid ASCs can create synergistic effects, such as improved charge transfer and enhanced electrochemical kinetics, leading to superior overall performance [6]. Three types of common hybrid ACSs are metal oxide/carbon composites, conductive polymer/carbon composites, and metal oxide/conductive polymer composites [7-9]. Among these, metal oxide/graphene composite materials have shown great potential as electrode materials for high-performance hybrid ACSs. Metal oxides, such as RuO_2, MnO_2, and NiO, have been widely investigated as pseudo capacitive materials due to their high redox activity and excellent theoretical capacitance. On the other hand, graphene, with its high electrical conductivity and vast surface area, has been extensively used as a conductive support and capacitive material in supercapacitor electrodes. The merge of metal oxides and graphene in composite materials has shown great promise for hybrid asymmetric supercapacitor applications. The synergistic effects between the metal oxide and graphene components can improve electrochemical performance, including enhanced capacitance, rate capability, and cycling stability [8]. In a study reported by Mao et al., a $NiCo_2O_4$/ GO composite and N-doped graphene were

[DOI: 10.22068/ijmse.3791]

synthesized. An asymmetric supercapacitor with high voltage was successfully constructed utilizing the $NiCo_2O_4$/GO composite as the positive electrode and N-doped graphene as the negative electrode. This asymmetric supercapacitor achieved an impressive energy density of 34.4 Wh kg^{-1} at 800 W kg^{-1} and maintained a capacity of 28 Wh kg^{-1} even at a power density of 8000 W kg^{-1} [10]. Zhang et al. fabricated a 3D- rGO/C/MnO_2 nanocomposite. They constructed a solid-state asymmetric supercapacitor using rGO/C/MnO_2 and activated carbon (AC) as the positive and negative electrodes, respectively, and a gel electrolyte composed of polyvinyl alcohol (PVA) and LiCl. This device achieved a remarkable power density of 3.6 kW kg^{-1} at a current density of ~3.2 A g^{-1} and an impressive energy density of 21.2 Wh kg^{-1} at a current density of ~0.16 A g^{-1}. Additionally, two rGO/C/MnO_2//AC ASCs connected in series could light a commercial LED for over 40 seconds [11]. Shao et al. presented a straightforward approach for creating flexible, self-supporting, 3D-porous graphene/MnO_2 nanorod and graphene/Ag hybrid thin-film electrodes through a filtration assembly technique. These graphene hybrid films enhance ion and electron transport by reducing ion-transport resistances and shortening diffusion distances, resulting in high specific capacitances, impressive power performance, and excellent mechanical flexibility. They developed an innovative asymmetric supercapacitor using a graphene/ MnO_2 nanorod thin film as the positive electrode and a graphene/Ag thin film as the negative electrode. These devices achieve a peak energy density of 50.8 Wh kg^{-1} and demonstrate a high power density of 90.3 kW kg^{-1}, even at an energy density of 7.53 Wh kg^{-1} [12]. Meng et al. developed a novel asymmetric supercapacitor utilizing α-Fe_2O_3/rGO nanocomposites as the negative electrode and α-MnS/rGO nanocomposites as the positive electrode. The resulting α-MnS/ rGO//α-Fe_2O_3/rGO ASCs exhibited an impressive voltage window of 1.6 V in 3 M KOH electrolyte. This supercapacitor achieved a maximum specific capacitance of 161.7 Fg^{-1} at a current density of 1 Ag^{-1} and a notable energy density of 57.5 Wh kg^{-1} at a power density of 800 W kg^{-1}. The remarkable performance of the α-MnS/rGO//α-Fe_2O_3/rGO supercapacitors highlights the potential of α-Fe_2O_3/rGO and α-MnS/rGO nanocomposites as excellent candidates for ASCs applications [13]. These reports demonstrate the effectiveness of metal oxide/graphene composite materials in enhancing the performance of ASCs, with improved power density, energy density, and specific capacitance compared to individual components. The synergistic effects between the metal oxide and graphene components are crucial in achieving these superior electrochemical properties.

In this work, we configured the asymmetric hybrid supercapacitor using the rGO/α-Fe_2O_3 nanocomposite as the negative electrode and the rGO/TiO_2 nanocomposite as the positive electrode. These two nanocomposites were produced using an easy and economical hydrothermal technique, and after characterizing their microstructure and morphology, their electrochemical performance was investigated.

2. EXPERIMENTAL PROCEDURES

All chemical substances utilized in this study were analytical grade (Merck, analytical grade). In the Hummers method, graphite powder served as the precursor for graphene oxide (GO), while phosphoric acid (H_3PO_4), potassium permanganate ($KMnO_4$), hydrogen peroxide, and sulfuric acid (H_2SO_4, 98%) acted as strong oxidizers. Acetone, ethanol, deionized (DI) water, and hydrochloric acid (HCl) were used for washing. Iron (III) nitrate [$Fe(NO)_3.9H_2O$] and urea (CH_4N_2O) were the precursors for α-Fe_2O_3, titanium tetraisopropoxide (TTIP) was the precursor for TiO_2, and potassium hydroxide (KOH) served as the electrolyte and nickel foam.

2.1. Preparation of rGO/α-Fe_2O_3 and rGO/TiO_2 Nanocomposite

The GO was produced through an enhanced Hummers method [14]. Then, both rGO/α-Fe_2O_3 and rGO/TiO_2 nanocomposites were synthesized in two steps. In the first step, graphene oxide was reduced using the hydrothermal method. In the second step, nanocomposites were synthesized using the in-situ hydrothermal method using rGO and iron and titanium precursors.

In the first step, 120 mg of GO was dispersed in 40 ml of deionized (DI) water for 1 hour in an ultrasonic bath (GRANT-17002), then it was poured into a 60 ml Teflon-lined autoclave and heated in an oven at 180°C for 12 hours. Then, the autoclave was taken out of the oven, and after it reached room temperature (RT), the rGO was

[DOI: 10.22068/ijmse.3791]

taken out and washed three times with DI water. In the subsequent step, to synthesize the rGO/α-Fe_2O_3 nanocomposite, 8 ml of a 5 mM $Fe(NO)_3.9H_2O$ solution and 60 mg of urea were mixed into 10 ml of a rGO suspension (2 mg mL^{-1}) while stirring. After 30 minutes, the mixture was transferred to a 40 mL Teflon-lined autoclave and heated in an oven at 180°C for 12 hours. Once the autoclave had cooled to room temperature, the resulting product was rinsed three times with deionized water and dried at 70°C in an oven to yield the rGO/α-Fe_2O_3 nanocomposite. To synthesize the rGO/TiO_2 nanocomposite, 0.4 ml of TTIP was gradually added to 10 ml of ethanol while stirring vigorously for one hour using an IKA Magnetic Stirrer (RCT basic). Next, 8 ml of the resulting mixture was slowly introduced to 20 ml of rGO suspension (2 mg mL^{-1}) and stirred for another hour. The mixture was then subjected to ultrasonic treatment for one hour (with a volumetric ratio of TTIP to GO suspension of 0.016). Subsequently, the mixture was transferred to a 50 ml autoclave and heated to 180°C for 12 hours. Finally, the autoclave was allowed to cool to room temperature, and the contents were washed three times with deionized water, followed by drying at 70°C in an oven to yield the rGO/TiO_2 nanocomposite.

2.2. Materials Characterization

X-ray diffractometry (XRD: PANalytical) was utilized with Cu Kα radiation at a current of 40 mA and an operating voltage of 40 kV to analyze the synthesized materials' structure, phase, and crystallinity. A field emission scanning electron microscope (FESEM) (MIRA3 TESCAN-XMU) was employed for the microstructural examination of the samples.

2.3. Electrochemical Measurements

To perform electrochemical tests, it is necessary to prepare a suitable electrode that can be used in a three-electrode cell. For this purpose, nickel foam was used due to its porous structure, which allows coating the electrode material, and its high electrical conductivity, which can also act as a current collector. Nickel foam was cut in measurements of 1.5 by 1.5 cm. Then, to eliminate potential contamination, the foam was washed in acetone and water for 5 minutes in an ultrasonic bath. Then, the foam was dried and weighed. 5 mg of the desired material was first dispersed in 2 ml of ethanol to coat the electrode material on the nickel foam. Then, the nickel foam was dipped in the solution and kept in it for a few seconds. Then, the foam was dried using hot air flow and weighed. This work was repeated several times until the weight of the electrode material coated on the foam was about 2-3 mg. This method prepared cathode and anode electrodes using nanocomposites rGO/TiO_2 and rGO/α-Fe_2O_3, respectively. The prepared cathode and anode were placed between two stainless steel sheets to assemble the hybrid asymmetric supercapacitor, and filter paper was used as a separator between the two electrodes. The assembly was tightly closed by plastic clamps and placed in 1 M KOH electrolyte. Cyclic voltammetry (CV) was conducted within a potential range of -1 V to 0 V for rGO/α-Fe_2O_3 and from 0 V to 0.65 V for rGO/TiO_2 at scan rates of 5, 10, 30, and 50 mV/s. Galvanostatic charge/discharge (GCD) tests were performed at various current densities within the same potential range. These experiments were carried out using an Auto-lab (PGSTAT 302N) and a three-electrode setup, which included a counter electrode (Pt wire), a reference electrode (Ag/AgCl), and a working electrode (Ni foam coated with rGO/α-Fe_2O_3 and rGO/TiO_2 nanocomposites). All electrodes were submerged in a 1 M KOH electrolyte.

3. RESULTS AND DISCUSSION

3.1. Structural and Microstructural Investigations of rGO/α-Fe_2O_3 and rGO/TiO_2 Nanocomposites

XRD analysis was employed to determine the crystalline structure of the nanocomposites. The diffraction pattern of nanocomposites is shown in Fig. 1a. For rGO/α-Fe_2O_3 sample, it can be seen that the peaks at 24.32°, 33.25°, 35.80°, 40.96°, 49.59°, 54.20°, 57.73°, 62.60°, and 64.21°, which are marked with crystalline planes of (012), (104), (110), (113), (024), (116), (018), (214) and (300) respectively, are entirely by the diffraction pattern of hematite with rhombohedral structure (reference number 000-03300664) [15, 16]. There is also a peak at 24.50°, which is related to the diffraction of (002) planes of rGO. For the rGO/TiO_2 sample, the observed peaks are entirely consistent with the diffraction pattern of anatase with a tetragonal structure (reference number 96-900-8214). Peaks at 25.58°, 38.02°, 48.00°,

[DOI: 10.22068/ijmse.3791]

54.04°, 55.33°, 62.99°, 68.87°, 70.50°, and 75.01° are identified respectively with crystalline planes of (101), (112), (200), (105), (211), (204), (116), (220), and (215). It should be noted that the diffraction peak of (002) crystal planes of rGO and (101) crystal planes of the anatase phase overlapped at 25.50°, which led to a broader peak [17, 18]. Fig. 1b, c, d, and e show the FESEM micrographs of rGO/TiO_2 and rGO/α-Fe_2O_3 nanocomposites in two magnifications. The formation of α-Fe_2O_3 and TiO_2 nanoparticles on the rGO sheets can be seen in these images. The formation of these spherical nanoparticles on the rGO sheets led to the wrinkling of the sheets and caused the rGO sheets to develop a porous structure.

3.2. Electrochemical Investigations of rGO/α-Fe_2O_3 and rGO/TiO_2 Nanocomposites

According to Fig. 2a, it is evident that the CV curves (especially at low scan rates) are not entirely rectangular, which indicates that quasi-capacitance behavior is also present in this nanocomposite. Within the voltage range of -1 to -0.5 V, two oxidation peaks and one reduction peak are detected, resulting from the reversible reaction between Fe^{3+} and Fe^{2+}. The oxidation peak at -0.8 V corresponds to the creation of $Fe(OH)_2$, while the peak near -0.55 V is linked to the formation of FeOOH. The reduction peak observed at -0.9 V corresponds to the conversion of FeOOH into $Fe(OH)_2$ [19]. The intensity of these peaks decreases with increasing scan rate, which is attributed to electron transfer kinetics in the electrode materials. Generally, according to CV curves' shape, electric double layer and quasi-capacitance behavior are engaged in charge storage. However, considering the feeble peaks related to iron redox, it can be inferred that the role of electric double-layer formation in charge storage is more significant than that of quasi-capacitance behavior [20]. As can be seen, the surface area of the CV curves expands with an increase in the scan rate, which confirms the capacitive behavior and the swift diffusion of electrolyte ions into the surface of the electrode material. As the scan rate increases, the specific capacity decreases. At slow scan rates, electrolyte ions have sufficient time to access the active sites within the electrode material. Conversely, at elevated scan rates, only the active sites on the surface can engage in electrochemical reactions. According to Formula 1, the specific capacity of rGO/α-Fe_2O_3 nanocomposite was calculated at various scan rates, and the findings are illustrated in Fig. 2b.

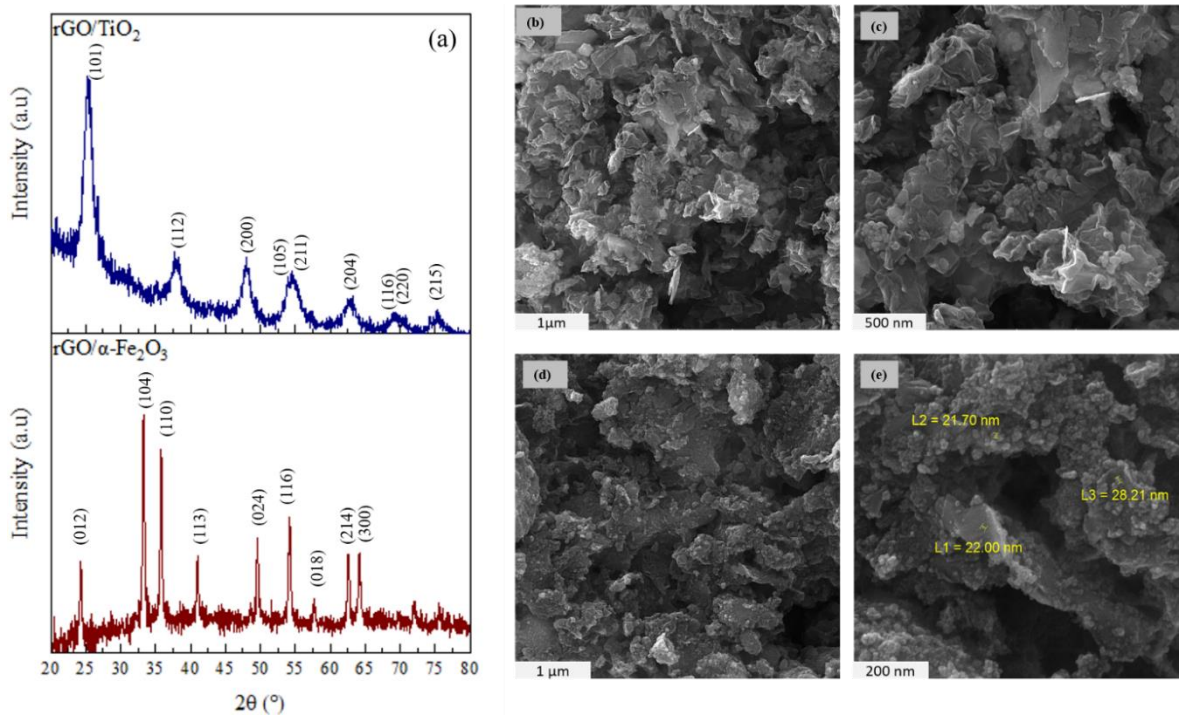

Fig. 1. a) XRD patterns of rGO/α-Fe_2O_3 and rGO/TiO_2 nanocomposites, b) and c) FESEM images of rGO/α-Fe_2O_3 and d) and e) FESEM images of rGO/TiO_2 nanocomposites

[DOI: 10.22068/ijmse.3791]

$$C = \frac{1}{2m\upsilon\Delta V}\int idV \quad (1)$$

Where υ is the scan rate (V. s^{-1}), m is the mass (g) of the electrode, ΔV is the potential window (V), i is the current (A), and ∫idV is the integration area for the CV curves [21]. The maximum specific capacity was achieved at scan rates of 5 mV/s, 130 F/g.

GCD analysis of rGO/α-Fe_2O_3 nanocomposite was measured in the potential range of -1 to 0 V at the current density of 1, 5, and 10 A/g. According to Fig. 2c, it is evident that the shape of all the charge/discharge curves diverges from the isosceles triangle (which is related to the pure electrical double-layer capacitance behavior). Similar to the results of CV, the results of GCD also confirm the existence of Faradic reactions in the charge storage process. Curve GCD shows that redox reactions happen from -1 to -0.4 V. Also, the voltage drop due to the series resistance is observed at the start of the discharge process, indicating the electrode's internal resistance [19]. Fig. 2d shows the CV curves of rGO/TiO_2 nanocomposite at scan rates of 5, 10, 30, and 50 in the voltage window of 0 to 0.65 V. As can be seen, a couple of redox peaks can be seen in the CV curve, which indicates the presence of the Faradic mechanism in charge storage. In addition, a partial part of the double-layer mechanism also contributes to charge storage. Fig. 2e shows the results of the specific capacitance of the rGO/TiO_2 nanocomposite, which, at 5 mV/s scan rate, the value of the specific capacitance is 253 F/g [22]. According to Fig. 2f, it is clear that the shape of all charge/discharge curves diverges from the isosceles triangle. Therefore, GCD results also confirm the existence of faradic reactions in the charge storage mechanism. According to the curve, redox reactions happen in the 0.2 to 0.4 V range.

3.3. Electrochemical Investigations of rGO/α-Fe_2O_3//rGO/TiO_2 Hybrid Asymmetric Supercapacitor

Electrochemical investigations of the two-electrode system, including rGO/α-Fe_2O_3 nanocomposite as anode and rGO/TiO_2 nanocomposite as cathode, were performed in 1 M KOH electrolyte. CV analysis was used to find the working potential window of the assembled ASC. This analysis increased the potential window with 0.2 V steps from 1 to 1.6 V, and CV curves were recorded at a 50 mV/s scan rate. Fig. 3a shows the resulting CV curves. It can be seen that with the gradual increase of the potential window, the CV curve becomes more extended, and the cathodic and anodic peaks appear. According to the curves in Fig. 3a, 1.6 V was considered the working potential of the rGO/α-Fe_2O_3// rGO/TiO_2 Hybrid asymmetric supercapacitor.

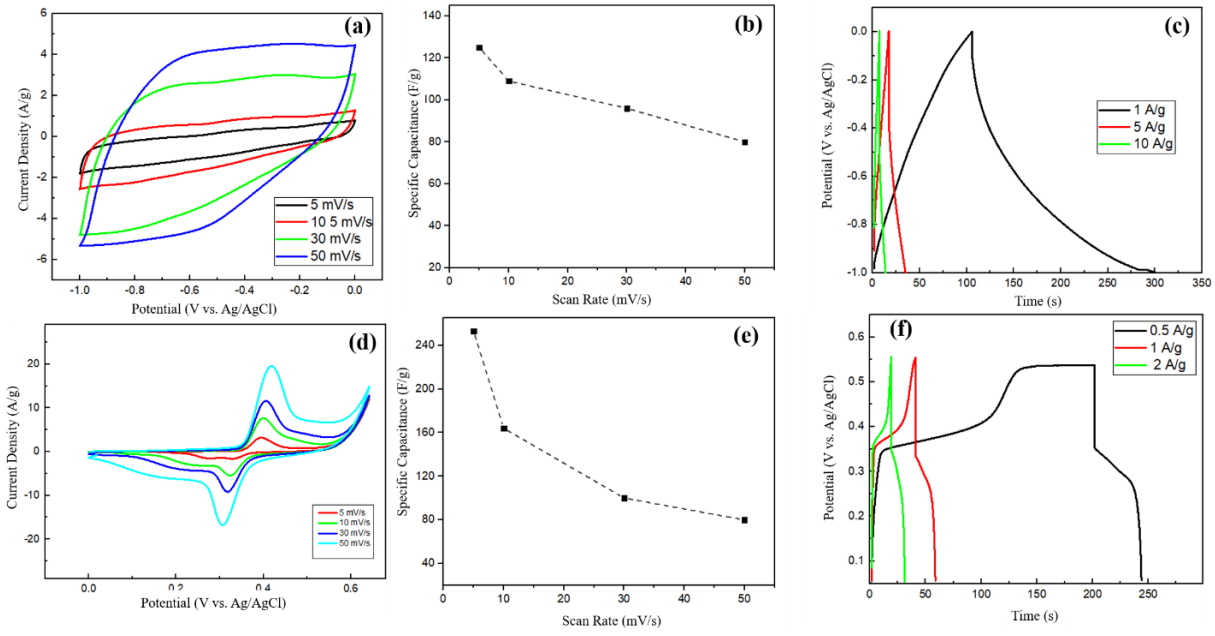

Fig. 2. a) CV curves, b) the specific capacitance versus the scan rate, c) GCD curves for rGO/Fe_2O_3 nanocomposite, d) CV curves, e) the specific capacitance versus the scan rate and f) GCD curves for rGO/TiO_2 nanocomposite

[DOI: 10.22068/ijmse.3791]

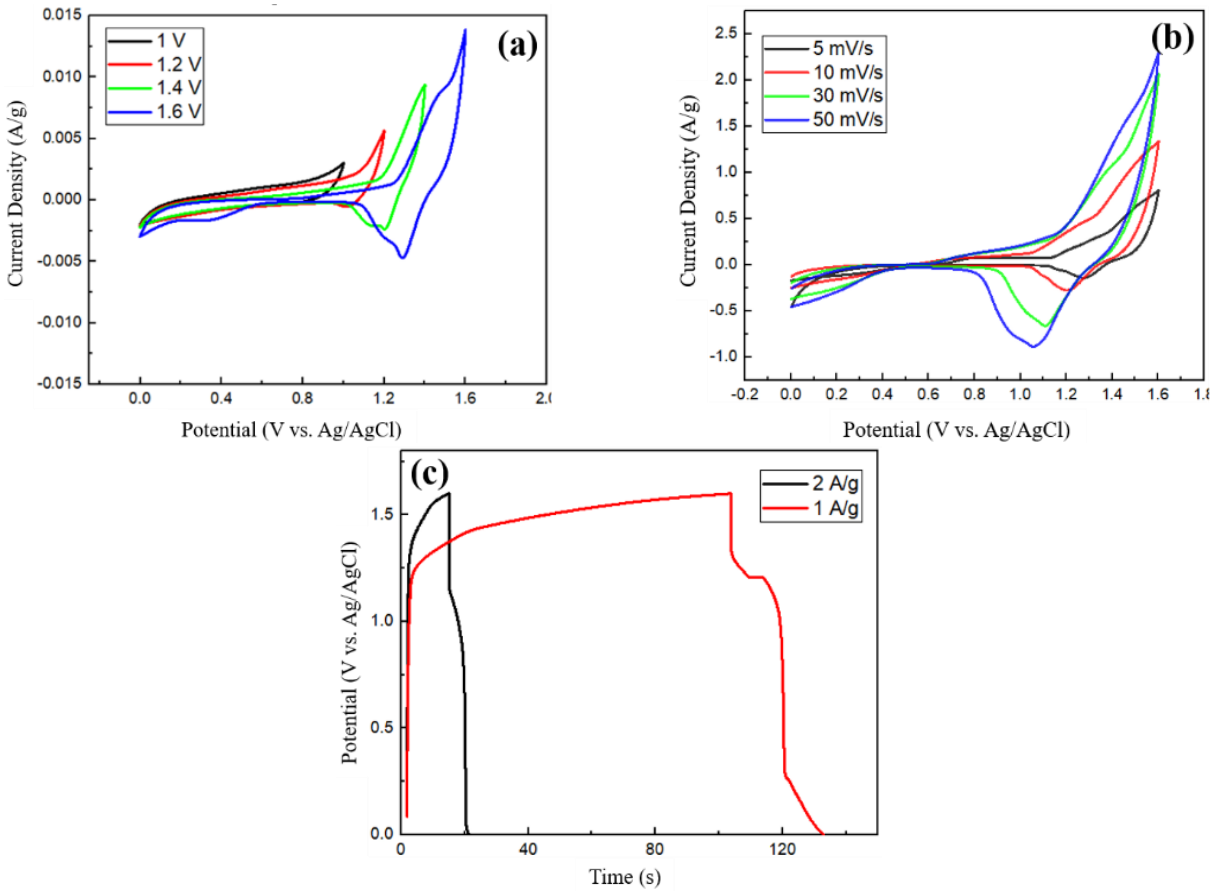

Fig. 3. CV curves of hybrid ASC a) in the working potential window of 1, 1.2, 1.4, and 1.6 V at a 50 mV/s scan rate, b) in the working potential window of 1.6 V at scan rates 5, 10, 30, and 50 mV/s, c) GCD curves of asymmetric supercapacitors at 1 and 2 A/g current densities

Fig. 3b reveals the CV curves of asymmetric supercapacitors in the working potential window of 1.6 V at 5, 10, 30, and 50 mV/s scan rates. At all scan rates, cathodic and anodic peaks are observed, indicating a quasi-capacitive behavior in the charge storage mechanism of the electrodes [23, 24]. At high scan rates, it can be seen that the CV curve becomes more extended, and the current density increases significantly. Also, anodic peaks are shifted to lower voltages, and cathodic peaks are shifted to higher voltages. Fig. 3c shows the GCD curves at 1 and 2 A/g current densities. It can be seen that the discharge time is less than the charging time of the asymmetric supercapacitor. Also, the voltage drop is caused by the equivalent series resistance observed at the beginning of the discharge, which indicates the internal resistance of the electrode, which seems to be attributed to the presence of metal oxide nanoparticles in the electrode material.

Table 1 summarizes key parameters from recent studies on asymmetric supercapacitors. Compared to conventional configurations, our rGO/α-Fe_2O_3// rGO/TiO_2 system demonstrates competitive energy storage metrics, achieving a potential window of 1.6 V and a power density of 1066 W kg^{-1}.

4. CONCLUSIONS

In this work, the rGO/α-Fe_2O_3 and rGO/TiO_2 nanocomposites were achieved via a facile hydrothermal technique, which enables the uniform distribution of the metal oxide nanoparticles on the rGO sheets. The unique nanostructured architecture of these composites provides efficient ion transport pathways and improved electrochemical activity, leading to enhanced capacitive performance. Compared to symmetric supercapacitors, the hybrid ASC device was fabricated by pairing the rGO/α-Fe_2O_3 negative electrode with the rGO/TiO_2 positive electrode, allowing for an expanded working potential window and improved energy density.

[DOI: 10.22068/ijmse.3791]

Table 1. Key parameters from recent asymmetric supercapacitors

Asymmetric configuration	Fabrication Method	Power density (W. Kg^{-1})	Potential window (V)	Ref.
$Fe_2O_3/NiCo_2O_4$/rGO-//Co_3O_4	Hydrothermal, Freeze drying	354.8	1.2	[25]
α-Fe_2O_3/hierarchical porous carbon (HPC)//PANI/HPC	Hydrothermal	1000	2.0	[26]
TiO_2-30% CuO// activated carbon	Low-cost wet chemical method	800	1.6	[27]
3DG–SnO_2–TiO_2//AC	Hydrothermal	367.7	1.5	[28]
rGO/α-Fe_2O_3//rGO/TiO_2	Hydrothermal	1066	1.6	This work

The electrochemical measurements of the device, including CV and GCD, demonstrate the superior capacitive behavior, high rate proficiency, and impressive cycling stability of the developed hybrid ASC. The perfect performance can be due to the synergistic effects of the rGO matrix and the metal oxide nanoparticles, which enhance the charge storage mechanisms and facilitate efficient ion and electron transport. The results of this work provide precious insights into the design and development of high-performance asymmetric supercapacitors with tailored nanocomposite electrodes, smoothing the way for their potential applications in energy storage devices and power delivery systems.

ACKNOWLEDGEMENTS

The authors would like to acknowledge the Research and Technology deputy of Sharif University of Technology for supporting this research (Grant number: G4000301).

REFERENCES

[1]. Sadavar, S. V., Lee, S.Y., and Park, S.J., "Advancements in Asymmetric Supercapacitors: From Historical Milestones to Challenges and Future Directions". J. Advanced. Science. 2024, 2403172.

[2]. Qorbani, M, Chen, K.H., and Chen, L.C., "Hybrid and Asymmetric Supercapacitors: Achieving Balanced Stored Charge across Electrode Materials". J. Small, 2024, 2400558.

[3]. Xu, Y., Lin, Z., Zhong, X., Huang, X., Weiss, N. O., Huang, Y., and Duan, X. "Holey graphene frameworks for highly efficient capacitive energy storage". J. Nature communications, 2014, 5(1), 1-8.

[4]. Wang, G., Zhang, L., and Zhang, J. "A review of electrode materials for electrochemical supercapacitors". J. Chemical Society Reviews, 2012, 41(2), 797-828.

[5]. Augustyn, V., Simon, P., and Dunn, B., "Pseudo capacitive oxide materials for high rate electrochemical energy storage". J. Energy & Environmental Science, 2014, 7(5), 1597-1614.

[6]. Zhu, J., Xu, Y., Chen, J., Lu, Y., and Jiang, L., "Reduced graphene oxide/α-Fe_2O_3 composite as a high-performance anode material for sodium-ion batteries". J. ACS applied materials & interfaces, 2015, 7(21), 11174-11182.

[7]. Simon, P., and Gogotsi, Y., "Materials for electrochemical capacitors". J. Nature materials, 2008, 7(11), 845-854.

[8]. Stoller, M. D., and Ruoff, R. S., "Best practice methods for determining an electrode material's performance for ultracapacitors". J. Energy & Environmental Science, 2013, 3(9), 1294-1301.

[9]. Zomorodian Esfahani, M, Soroush, E, Mohammadnejad, S, Helli, M, Malek Khachatourian, A., Toprak, S. and Varma, R, S., "Copper oxide/graphene-based composites: Synthesis methods, appliances and recent advancements". J. FlatChem., 2024, 47, 2452-2627.

[10]. Mao, J.W., He, C.H., and Qi, J.Q. "An Asymmetric Supercapacitor with Mesoporous $NiCo_2O_4$ Nanorod/Graphene Composite and N-Doped Graphene Electrodes". J. Electron. Mater, 2018, 47, 512–520.

[11]. Zhang, H, Lin, L, Wu, B, and Hu, N, "Vertical carbon skeleton introduced three-dimensional MnO_2 nanostructured composite electrodes for high-performance asymmetric supercapacitors". J. Power Sources, 2020, 476, 228527.

[12]. Shao, Y., Wang, H., Zhang, Q., and Li, Y., "High-performance flexible asymmetric

[DOI: 10.22068/ijmse.3791]

supercapacitors based on 3D porous graphene/MnO_2 nanorod and graphene/Ag hybrid thin film electrodes". J. Materials Chemistry C, 2013, 1(6), 1245-1251.

[13]. Meng, J., Wang, Y., and Xie, X., "High-performance asymmetric supercapacitor based on graphene-supported iron oxide and manganese sulfide". J. Ionics, 2019, 25, 4925–4933.

[14]. Chen, J., Yao, B., Li, C., and Shi G., "An improved Hummers method for eco-friendly synthesis of graphene oxide". J. Carbon, 2013, 64(1), 225–229.

[15]. Justus, J. Sharmila, S. Dawn Dharma Roy, and A. Moses Ezhil Raj., "Synthesis and characterization of hematite nanopowders". J. Materials Research Express, 2016, 3.10, 105037.

[16]. Abasali karaj abad, Z., Nemati, A., Malek Khachatourian, A., "Synthesis and characterization of rGO/Fe_2O_3 nanocomposite as an efficient supercapacitor electrode material". J. Mater Sci: Mater Electron, 2020, 31, 14998–15005.

[17]. Thamaphat, K, Limsuwan, P, and Ngotawornchai. B., "Phase characterization of TiO_2 powder by XRD and TEM". J. Agriculture and Natural Resources, 2008, 42.5, 357-361.

[18]. Abasali Karaj Abad Z, Nemati A, Malek Khachatourian A, Golmohammad M. "The Effect of Pre-reduction of Graphene Oxide on the Electrochemical Performance of rGO-TiO_2 Nanocomposite". J. IJMSE, 2020, 17 (4), 55-61.

[19]. Radić, G., Šajnović, I., Petrović, Ž., and Kraljić Roković, M., "Reduced graphene oxide/α-Fe_2O_3 fibres as active material for supercapacitor application". J. Croatica chemica acta, 2018, 91.4, 481-490.

[20]. Carminati, S. A., Souza, F. L., and Nogueira, A. F., "Enhancing hematite photoanode activity for water oxidation by incorporation of reduced graphene oxide". J. ChemPhysChem, 2016, 17.1, 170-177.

[21]. Joshi, P.S., and Sutrave, D.S., "A brief study of cyclic voltammetry and electrochemical analysis". J. ChemTech Res, 2018, 11(9), 77–88.

[22]. Anandhi, P, Harikrishnan, S, Senthil Kumar, V.J., Lai, W.C., and Mahmoud, A.E.D., "The enhanced energy density of rGO/TiO_2 based nanocomposite as electrode material for supercapacitor". J. Electronics, 2022, 11, 1792.

[23]. Sharma, S, and Chand, P, "Supercapacitor and electrochemical techniques: A brief review". J. Results in Chemistry, 2023, 5, 100885.

[24]. Nazari, N, Dehghani Mohammad Abadi, M, Khachatourian, A.M., Golmohammad, M, and Nemati, A, "The effect of phosphorus and nitrogen dopants on structural, microstructural, and electrochemical characteristics of 3D reduced graphene oxide as an efficient supercapacitor electrode material". J. Diamond and Related Materials, 2023, 137, 110-114.

[25]. Yuan, B, An, Zh, Chen, L, Luo, Sh, Wang, X, and Zhang, Ch, "Application of Fe-based nanocomposites for the preparation of high-performance asymmetric supercapacitors". J. Electrochimica Acta, 2024, 497, 144585-144598.

[26]. Pingping, Y, Wei, D, and Yanfeng, J, "Porous Fe_2O_3 Nanorods on Hierarchical Porous Biomass Carbon as Advanced Anode for High-Energy-Density Asymmetric Supercapacitors". J. Frontiers in Chemistry, 2020, 8, 611852-611861.

[27]. Zia Ullah Shah, M, Sajjad, M, Hou, H, Rahman, Sh, Mahmood, A, Aziz, U, and Shah, A, "A new CuO/TiO_2 nanocomposite: An emerging and high energy efficient electrode material for aqueous asymmetric supercapacitors". J. Journal of Energy Storage, 2022, 55, 105492-105505.

[28]. Zamiri, G, Haseeb, A.S. Md., Jagadish, P, Khalid, M, Kong, I, and Krishnan, S.G, "Three-Dimensional Graphene–TiO_2–SnO_2 Ternary Nanocomposites for High-Performance Asymmetric Supercapacitors". J.ACS Omega, 2022, 48, 43981–43991.

[DOI: 10.22068/ijmse.3791]